UNDERSTANDING LOCALIZED CORROSION PROPERTIES AT ELEVATED CHLORIDE CONCENTRATION AND TEMPERATURE

R. M. Katona[1] and R. G. Kelly[1]

[1] Materials Science and Engineering, University of Virginia, Charlottesville, VA 22904 USA

Key words: stainless steel, pitting corrosion, 1D artificial pit, elevated temperature

Abstract

Key factors leading to the determination of a maximum pit size for stainless steel 304L (SS304L) are presented for atmospheric conditions with elevated chloride concentrations and temperatures. This evaluation was carried out by experimentally determining the pit stability product ($(i \cdot x)_{sf}$) and repassivation potential (E_{rp}). Overall, it was found that $(i \cdot x)_{sf}$ decreases with increasing chloride concentration and increases with increasing temperature. E_{rp} was determined to decrease with increasing concentration and increase with increasing temperature.

Introduction

Type 300 stainless steels (SS) are used heavily in marine environments due to their overall corrosion resistance.[1] Characterized as a corrosion resistant alloy, the passive oxide on 300 grade SS, specifically SS304L, is susceptible to localized corrosion in the presence of an aggressive anion species, including chloride which is the dominant anion in marine atmospheres. Localized corrosion is a metastable process which is governed by the alloying elements in the sample of interest, the bulk environment (including oxidizing potential) and the critical chemistry within the pit cavity.[1]

Pitting corrosion involves spatially localized metal oxidation creating metal cations in the pit cavity which results in aggressive chemistries due to hydrolysis reactions.[1] The critical condition for pit stability has been given as the need to exceed the pitting potential (E_{pit}) and further the critical condition for propagation has been described by need to exceed the repassivation potential (E_{rp}) and the pit stability product ($i \cdot x$) where i is current density and x is pit depth.[2] E_{pit} is the potential above which stable pitting is discernible for a given alloy and environment while E_{rp} is a lower bound of electrochemical potential below which propagation will no longer occur and the pit will repassivate.[2] Galvele originally showed that for a one-dimensional pit to sustain dissolution, the quantity ($i \cdot x$) must exceed a critical value.[3] Stability is a battle between the production of acidity (via hydrolysis of metal cations produced by the dissolution current density, *i*) and diffusion of that concentrated solution to the bulk, which is controlled by the diffusion distance, *x*. Thus, a shallow pit requires a high current density to maintain stability, whereas a deep pit requires lower current density.

E_{pit} is dependent on experimental conditions as well as experimental technique causing a wide scatter in literature values.[2] However, assuming that a pit is actively growing on the surface, the growth phenomenon can be explained by transport phenomena and includes competitive adsorption, salt formation, film contamination among other phenomenon.[3] An original model developed by Pickering and Frankenthal,[4] exploited a one-dimensional pitting situation in which diffusion of metal cations from a pit was considered.

However, this model could not be applied in its original form to all pitting cases because it would lead to an increase in pH in the pit as it grew. This model was improved by Galvele and a summary is provided below.[3]

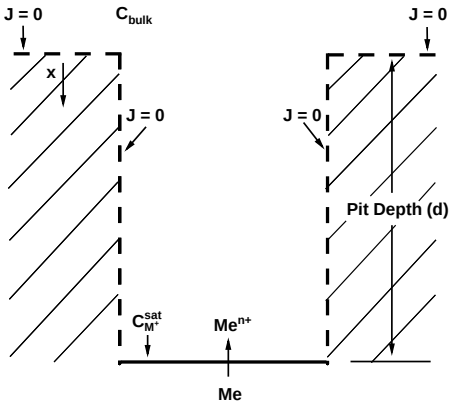

Figure 1: 1-Dimensional diffusion model exploited by Galvele formulism. It is pointed out in the original formulism that a saturation concentration was not required on the surface of the alloy for the original determination of the pit stability product and is further discussed in the introduction section. This figure is adapted from the original work of Galvele.[3]

As seen in Figure 1, Galvele used a geometry in which an active corroding metal was surrounded by a passive surface which was not undergoing corrosion.[3] That is, there is a flux (J) of metal ions from the metal surface at the bottom of the pit with no flux from the passive walls surrounding. When a metal undergoes anodic dissolution, a general expression for the anodic reaction taking place can be given by,

$$Me = Me^{n+} + ne^{-} \qquad (1)$$

where Me is the metal of interest, in this case is SS304, and n is the number of electrons transferred during the anodic dissolution.[5] Based on stoichiometric dissolution of the alloy used in this study, $n_{304} = 2.2$.[6] The reaction given in Equation (1) is assumed to occur in a given aggressive sodium salt solution with a non-complexing anion. The metal dissolution is then followed by hydrolysis in the pit given by

$$Me^{n+} + H_2O \leftrightarrow Me(OH)^{(n-1)} + H^{+} \qquad (2)$$

causing a decrease in pH in the pit.[3] The transport of these metal ion in solution at steady state can be modeled by Fick's first law and is given by

$$i = \frac{nFD_{M^+}\Delta C}{d} \qquad (3)$$

where i is the current density of anodic dissolution, F is Faraday's constant $\left(F = 96{,}485\frac{C}{mol}\right)$, D_{M^+} is the average metal ion diffusivity, ΔC is the concentration gradient of metal cations in solution, and d is the depth of the pit of interest. This equation can be rearranged in order to yield the pit stability product given by,

$$id = nFD_{M^+}\Delta C = (i \cdot x) \qquad (4)$$

It is noted that Galvele's original formulism did not include the presence of a salt film on the surface of the alloy which will be discussed in the subsequent paragraph. Thus, by considering the transport of ionic species in and out of the pit, the determination of the critical value $(i \cdot x)$ can be achieved. This pit stability product can be interpreted in the following way: if at a certain depth (x) the anodic dissolution current density (i) is insufficient to meet the pit stability criterion, the pit will repassivate because the critical chemistry will be lost to the bulk by diffusion. Experimentally this geometry can be exploited by a lead-in-pencil configuration seen in Figure 2. By mounting a thin wire in a non-conductive epoxy, the diffusion situation in Figure 1 can be created.

Galvele's original formulism only accounted for the diffusion of cations in solution and did not account for any complexation in the solution.[3] It was later found out that pits propagating on the surface of an alloy can be

under the presence of a metal salt film on the pit surface.[2] That is, when metal ions in solution reach a critical concentration, the metal ions combine with chloride anions in solution and precipitate, forming a dynamic metal-chloride salt complex on the surface of the dissolving alloy. This situation provides for a limiting current density i_{lim} of metal cations through the salt film and changes the formulism of Equation (4) to the following:

$$i_{lim}d = nFD_{M^+}C_{M^+}^{sat} = (i \cdot x)_{sf} \quad (5)$$

where $C_{M^+}^{sat}$ is the saturation concentration of metal cations and the subscript sf denotes the presence of a salt film on the surface of the alloy.[2,6] This formulism will be exploited in experimentation. Along with this notation change, it is also noted that this critical valid is for a 1-D geometry. The value of $(i \cdot x)_{sf}$ can be converted to a 3-D hemispherical geometry, which is more realistic of atmospheric corrosion, and is based on the geometric flux from a corroding pit.[7]

Another important distinction to make with the presence of a salt film on the surface of the alloy is the morphology after propagation. The presence of a salt film can change the mode of propagation and can range from a smooth propagation under full saturation to etched pits under non-saturated conditions. Experimental evidence has also shown that pits can propagate when there is not complete saturation of a salt film on the surface of an alloy.[8] The degree of saturation on the surface of an alloy has been under great scrutiny and can range from 50-80% of saturation concentration.[2,9]

In lead-in-pencil experiments, the limiting current density is not truly one dimensionally diffusion limited at all pit depths.[5] Srinivasan et al. exploited finite element modeling in order to calculate the flux of metal cations in solution as a function of pit depth. It was found that for pit depths shallower than 8-10 times the width of the wire used, a flux which was consistently lower than analytically determined calculations for 1-D Fickian diffusion was observed. This deviation was due to substantial contribution of the external hemispherical boundary layer to the overall diffusion length. Increasing the pit diameter resulted in a larger boundary layer, which in turn affected the flux characteristics to greater depths.[5] Thus, in order to elucidate critical pitting parameters in a 1-D geometry, the artificial pit needs to be sufficiently deep.

Critical factors for localized corrosion have been explored at low temperatures or low chloride concentrations.[6,10] Although useful for certain applications, SS304L is subjected to marine environments that are characterized by high chloride concentrations (up to saturation) at high temperatures. Therefore, critical factors for localized corrosion will be explored at elevated chloride concentrations and temperatures.

Experimental

Artificial pit set-up: The pit stability product under the presence of a salt film $(i \cdot x)_{sf}$ and repassivation potential (E_{rp}) were determined for stainless steel 304L (SS304L) in four sodium chloride (NaCl) concentrations (0.6, 1, 3, 5.5 M). Solutions were temperature-controlled with a water bath at four temperatures (25°C, 35°C, 45°C, and 55°C) with an accuracy of $\pm$0.1°C. The composition by certificate of the SS304L wire used can be seen in Table 1. The diameter of the SS304L wire was 50 μm. The wire was embedded in epoxy so that the diameter of the wire was exposed with an area of $7.85E10^{-5}$ cm^2. An example of this set up can be seen schematically in Figure 2. The epoxy and wire were wet ground with 320 grit silicon carbide paper. The wires were examined under an optical microscope in order to ensure a cross-section of the wire was fully exposed. Prior to electrochemical testing, the samples were

Table 1: Composition of Stainless Steel 304L (all values reported in weight percent)

C	Mn	P	S	Si	Cr	Ni	Fe	Co	Nb	Ta	N
0.03	1.59	0.036	0.001	0.27	18.48	9.20	70.26	0.13	0.001	0.001	0.001

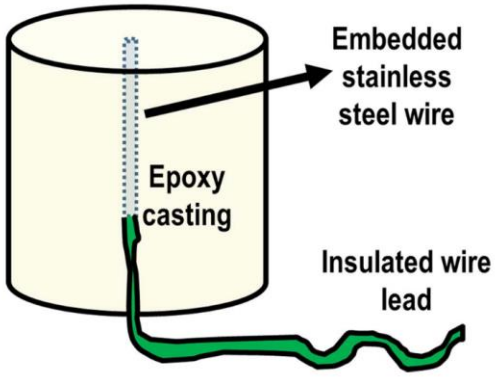

Figure 2: Schematic of lead-in-pencil configuration. The figure was obtained from the work of Srinivasan et al.[12]

further cleaned with methanol and dried in nitrogen.

Electrochemical technique: Samples were placed in an electrochemical cell and electrochemical testing was carried out by applying an anodic potential of +750 mV_{SCE} (versus a saturated calomel electrode (SCE)) for 5 to 20 minutes to ensure pit initiation with a platinum coated niobium mesh as a counter electrode. The potential was stepped down to +450 mV_{SCE} for different periods of time to allow for pit propagation to different depths. A polarization scan from +450 mV_{SCE} to -600 mV_{SCE} at a scan rate of 5 mV/sec was then carried out. After the polarization scan, the pit was immediately re-initiated by polarization to +750 mV_{SCE} and the cycle was repeated. A schematic representation of this sequence can be seen in Figure 3. Eight to ten repetitions of the cycle were performed as it has been shown that the pit depth needs to exceed 8-10 times the diameter (~400-500 μm) to prevent measured values from being influenced by the hemispherical diffusion at the pit mouth.[5] It is noted that pitting did not always initiate on the first cycle, and a higher potential was sometimes utilized to initiate pitting.

Determination of $(i \cdot x)_{sf}$*:* Successive polarization scans allow for the extraction of the limiting current density (i_{lim}) as well as E_{rp}, as a function of pit depth shown in Figure 4. Thus, based on Equation 5, plotting the limiting current densities against the reciprocal of the pit depth $(1/d)$ will determine $(i \cdot x)_{sf}$ via the slope of the curve. During the change in potential, the nominal change in current density was small and, therefore, the reaction was under diffusion-limited conditions at essentially a constant depth.

In order to determine the pit depth, the total anodic charge density during the potentiostatic holds and cathodic polarizations were converted to pit depth. Using Faraday's law for alloys, the depth of the pit can be expressed as:

$$d = \frac{A}{nF\rho} \int i \, dt \quad (2)$$

Where i is the current density, A is the mean atomic weight ($A_{304} = 55.3\ g/mol$), ρ is the density ($\rho_{304} = 7.8\ g/cm^3$), and dt are infinitesimal time steps.[11] These calculations were made assuming stochiometric dissolution of Fe^{2+}, Cr^{3+}, and Ni^{2+}. Automation of these calculations was carried out in Matlab R2017a with a method similar to that set forth by Srinivasan et al.[12]

Determination of E_{rp}*:* The value of the repassivation potential E_{rp} was determined by a computer script as the potential during the linear polarization scan at which the values of *Z%* of the next *N* current density data points in the scan were lower than 30 μA/cm^2. In the present study, *Z* and *N* were set to 70% and 30 points, respectively in accordance with Srinivasan et al.[12] This method serves as an

unbiased, rational means to determine when the potential has reached a relatively constant value, which is deemed E_{rp}. It is noted that no temperature corrections were made for E_{rp} measurements.

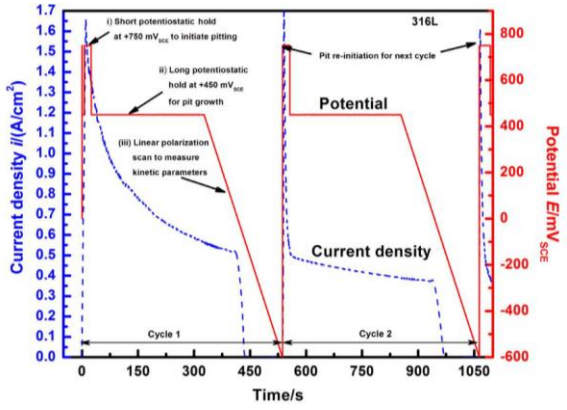

Figure 3: Schematic of electrochemical sequence employed for the determination of electrochemical parameters. The figure was obtained from the work of Srinivasan et al.[12]

Results

$(i \cdot x)_{sf}$ and $D_{M^+}C_{M^+}^{sat}$ in NaCl solutions: Figure 4 shows successive polarization scans of SS304L lead-in-pencil experiments which were used to determine the pit stability product ($(i \cdot x)_{sf}$) and repassivation potential (E_{rp}) as shown in Figure 5 (a) and (b) respectively. Pit depths on the order of 8-10 times the diameter of the wire were used in order to extract $(i \cdot x)_{sf}$. Assumptions of diffusion control during experimentation are validated by the observed linearity between i_{lim} and $(1/d)$ in Figure 5. Depths more shallow than 400 µm where ignored as there was a deviation from linearity indicating 1-dimensional diffusion control was no longer valid due to hemispherical diffusion in the bulk solution at the pit mouth.[5] Bulk NaCl solutions were used at their natural pH which ranged from 5.5-6.8. The same procedure was repeated across temperatures ranging from 25°C to 55°C with an accuracy of $\pm 0.1^{o}C$. The dependence of $(i \cdot x)_{sf}$ and $D_{M^+}C_{M^+}^{sat}$ with increased temperature in NaCl solutions can be seen in Figure 6(a) and (b) respectively. It is noted that $(i \cdot x)_{sf}$ and $D_{M^+}C_{M^+}^{sat}$ are directly related based on Equation 5. At all concentrations, an increase in $(i \cdot x)_{sf}$ and $D_{M^+}C_{M^+}^{sat}$ is seen with an increase in temperature. At all temperatures tested, $(i \cdot x)_{sf}$ decreased with increasing bulk NaCl concentration. Corresponding $D_{M^+}C_{M^+}^{sat}$ values can be seen in Figure 6(b) and again decrease with increasing bulk chloride concentration.

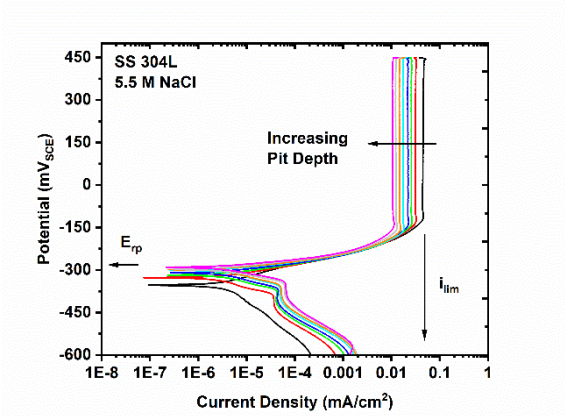

Figure 4: Successive polarization scans of SS304L in 5.5 M NaCl at T = 25°C after pit growth by anodic holds at both +750 mV$_{SCE}$ and +450 mV$_{SCE}$. Cathodic polarization was initiated at +450 mV$_{SCE}$ and scanned to -600 mV$_{SCE}$ at a scan rate of 5 mV/sec. Extraction of desired parameters, E_{rp} and i_{lim} are labeled. This set of polarization scans is representative of most lead-in-pencil experiments run in this experiment.

E_{rp} in NaCl solutions: The high-throughput method used in this study also allowed for the determination of E_{rp} which has been shown to be constant if sufficient charge was passed (*i.e.*, the pit was sufficiently deep).[13,14] An example of this can be seen in Figure 5(b) where data points with a charge density greater than 900 C/cm^2 were used to generate both an average and standard deviation. It is noted that the approach to a "plateaued" E_{rp} was not always via the same pattern. In Figure 5(b), E_{rp} increased with increasing charge density (deeper artificial pits). Other concentrations and temperature followed the opposite trend where increasing the charge density (deeper artificial pits) caused a decrease in E_{rp}. There

was no discernable pattern in concentrations or temperatures that lead to an ascension or depression to a plateaued E_{rp} value. This observation is similar to data reported by Woldemedhin et al. for lithium chloride (LiCl) solutions.[6] Overall, E_{rp} as a function of chloride concentration and temperature can be seen in Figure 7. Generally, with increased bulk NaCl concentration, a mild decrease in E_{rp} is seen. Subsequently, with an increase in temperature, E_{rp} increases. It is noted that the reported potentials are at the temperature of the solution. Despite standard deviations being large in comparison to $(i \cdot x)_{sf}$, performing a t-test on all bounding cases confirms the trends. For example, performing a t-test between 0.6 M and 5.5 M solutions at each temperature produces a p-value that is lower than an alpha value of α = 0.05 indicating the E_{rp} values are in fact different. However, significant differences were not always seen between 1M and 3M NaCl solutions. In terms of temperature, t-tests were performed between the same NaCl concentrations at temperatures 25°C and 55°C. All concentrations proved to be significantly different between 25°C and 55°C however, at 45°C and 55°C not all concentrations were significantly different suggesting E_{rp} is independent of temperature at the elevated temperatures tested in this experimentation.

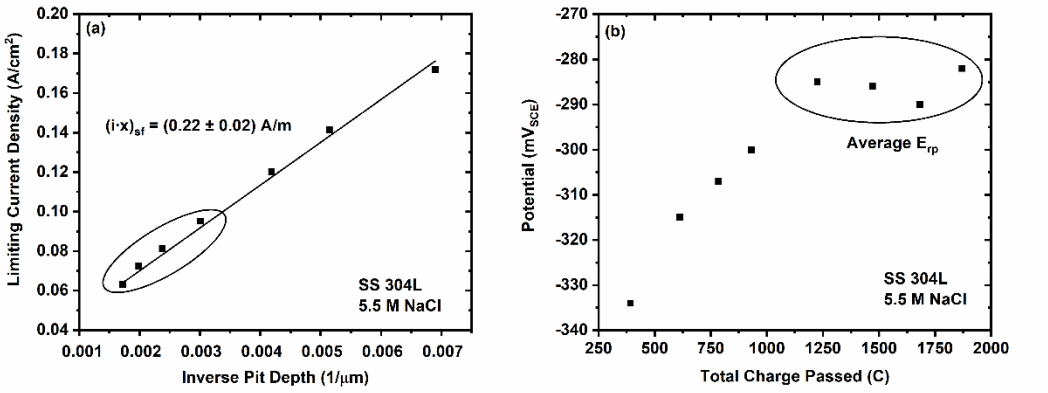

Figure 5: (a) Extraction of pit stability product $(i \cdot x)_{sf}$. It is noted that the x-axis is inverted pit depth in μm. Pits with a depth greater than 8 times the diameter of the pit were considered in the determination of pit stability product. (b) Extraction of the measured repassivation potential data at various pit depths. The E_{rp} value denoted is the plateau which the recorded values approach at deep pit depths/high charge density circled in the plot above. Data refer to 304L in bulk 5.5 M NaCl at T = 25°C.

Discussion

Anodic kinetics of stainless steel 304L in chloride-containing solutions were studied both as a function of chloride concentration and temperature. A high-throughput artificial pit method allowed for the extraction of pit stability product under the presence of a salt film ($(i \cdot x)_{sf}$) and the repassivation potential (E_{rp}). Anodic holds were used to grow one-dimensional pits in 50 μm diameter SS304L wire, and pit growth was followed by cathodic polarization to obtain these values. Kinetic data were obtained through successive anodic holds and cathodic scans. These results are summarized in Figure 6 and Figure 7 for $(i \cdot x)_{sf}$ and E_{rp} respectively. It is noted that $D_{M^+}C_{M^+}^{sat}$ will be used as a basis for discussion, however, is an equivalent expression to $(i \cdot x)_{sf}$ through the use the number of electrons transferred, and Faraday's constant as seen in Equation 5.

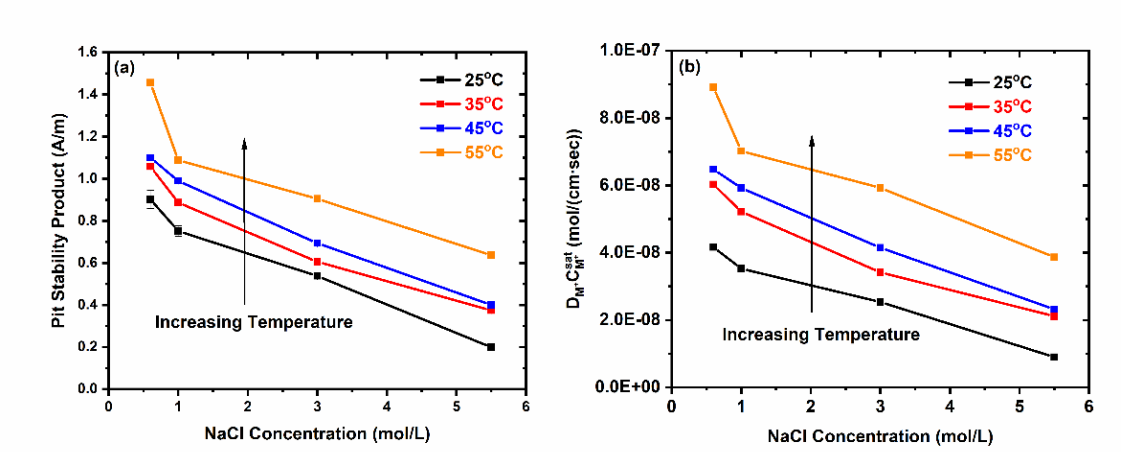

Figure 6: (a) Dependence of the pit stability product ($(i \cdot x)_{sf}$) on bulk sodium chloride concentration ([NaCl]) and temperature and (b) corresponding $D_{M^+}C^{Sat}_{M^+}$ values for stainless steel 304L. It is noted that error bars are included on all measurements, however standard deviation is smaller than the data point in some cases. Standard deviation is representative of at least 4 pit depths.

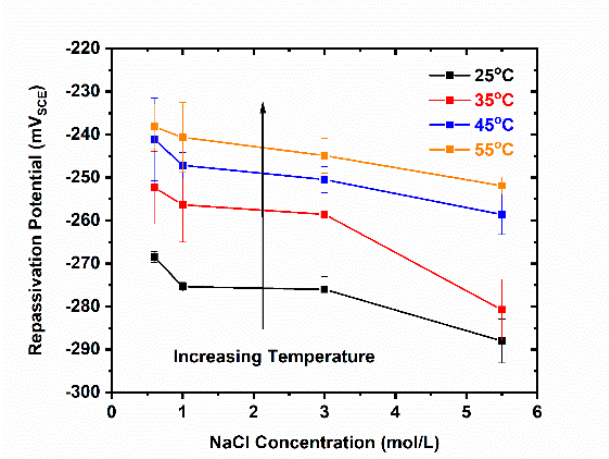

Figure 7: Dependence of repassivation potential on the bulk sodium chloride concentration ([NaCl]) and temperature on the pit stability product for Stainless Steel 304L. Reported temperatures have an accuracy of ±0.1°C and there is no temperature correction for the reference electrode.

$D_{M^+}C^{sat}_{M^+}$ decreases with increasing bulk chloride due to a decrease in saturation concentration and metal ion diffusivity: As shown in Figure 6(b), $D_{M^+}C^{sat}_{M^+}$ decreases with bulk chloride. The solubility of metal salts have been extensively shown for ferrous chloride solutions ($FeCl_2$).[15,16] The saturation of $FeCl_2$ has been used for the determination of saturation concentration for stainless steel alloys as the main component in the alloy is iron.[10,17] Thus, through the work of Ernst and Newman, an increase in bulk chloride concentration shows a decrease in the saturation concentration through the use of a solubility product.[17] Along with this, through the use of the Stokes-Einstein equation it has been shown that increasing bulk chloride concentration will also yield a lower metal ion diffusivity in solution. Thus, both D_{M^+} and $C^{sat}_{M^+}$ decrease with increasing bulk chloride therefore, the product $D_{M^+}C^{sat}_{M^+}$ will also decrease with increasing bulk chloride as shown in Figure 6(b).

$D_{M^+}C_{sat}$ increases as a function increasing temperature due to an increase in saturation concentration and metal ion diffusivity: Following the same logic as the previous paragraph, The saturation concentration has been shown to increase with increasing temperature.[15,16] This would also lead to an increase in metal ion diffusivity based on the Stokes-Einstein equation. Thus, both D_{M^+} and $C^{sat}_{M^+}$ increase with increasing temperature therefore, the product $D_{M^+}C^{sat}_{M^+}$ will also increase with increasing temperature as shown in Figure 6(b).

Conclusions

Pits stability product and repassivation potential were determined for elevated chloride concentrations and temperatures. 1-dimensional artificial pit electrodes were utilized to determine $(i \cdot x)_{sf}$, $D_{M^+}C_{M^+}^{sat}$, and E_{rp} in bulk NaCl solutions with concentrations of 0.6, 1, 3, and 5.5 M NaCl in controlled temperature environments of 25, 35, 45, and 55°C. Overall, with increasing bulk chloride concentration $D_{M^+}C_{M^+}^{sat}$ decreased. With an increase in temperature, an increase in $D_{M^+}C_{M^+}^{sat}$ occurred. E_{rp} was determined to decrease with increasing concentration and increase with increasing temperature.

References

1. McCafferty, E. *Introduction to Corrosion Science*. (2010).
2. Laycock, N. J. & Newman, R. C. Localised dissolution kinetics, salt films and pitting potentials. *Corros. Sci.* **39,** 1771–1790 (1997).
3. Galvele, J. R. Transport Processes and the Mechanism of Pitting of Metals. *J. Electrochem. Soc.* **123,** 464 (1976).
4. Pickering, H. W. & Frankenthal, R. P. On the mechanisms of localized corrosion of iron and stainless steel. *J. Electrochem. Soc.* **119,** 1297–1304 (1967).
5. Srinivasan, J., Liu, C. & Kelly, R. G. Geometric Evolution of Flux from a Corroding One-Dimensional Pit and Its Implications on the Evaluation of Kinetic Parameters for Pit Stability. *J. Electrochem. Soc.* **163,** C694–C703 (2016).
6. Woldemedhin, M. T., Srinivasan, J. & Kelly, R. G. Effects of environmental factors on key kinetic parameters relevant to pitting corrosion. *J. Solid State Electrochem.* **19,** 3449–3461 (2015).
7. Chen, Z. Y. & Kelly, R. G. Computational Modeling of Bounding Conditions for Pit Size on Stainless Steel in Atmospheric Environments. *J. Electrochem. Soc.* **157,** C69 (2010).
8. Woldemedhin, M. T., Shedd, M. E. & Kelly, R. G. Evaluation of the Maximum Pit Size Model on Stainless Steels under Thin Film Electrolyte Conditions. *J. Electrochem. Soc.* **161,** 3216–3224 (2014).
9. Srinivasan, J. & Kelly, R. G. One-Dimensional Pit Experiments and Modeling to Determine Critical Factors for Pit Stability and Repassivation. *J. Electrochem. Soc.* **163,** C759–C767 (2016).
10. Jun, J., Frankel, G. S. & Sridhar, N. Effect of chloride concentration and temperature on growth of 1D Pit. 1–9 (2015). doi:10.1007/s10008-015-2780-4
11. Gaudet, G. T. *et al.* Mass transfer and electrochemical kinetic interactions in localized pitting corrosion. *AIChE J.* **32,** 949–958 (1986).
12. Srinivasan, J., McGrath, M. J. & Kelly, R. G. A High-Throughput Artificial Pit Technique to Measure Kinetic Parameters for Pitting Stability. *J. Electrochem. Soc.* **162,** C725–C731 (2015).
13. Sridhar, N. & Cragnolino, G. A. Applicability of Repassivation Potential for Long-Term Prediction of Localized Corrosion of Alloy-825 and Type-316L Stainless-Steel. *Corrosion* **49,** 885–894 (1993).
14. Wilde, B. E. & Williams, E. The use of current/voltage curves for the study of localized corrosion and passivity breakdown on stainless steels in chloride media. *Electrochim. Acta* **16,** 1971–1985 (1971).
15. Chou, I. M. & Phan, L. D. Solubility Relations in the System Potassium Chloride-Ferrous Chloride-Water between 25 and 70C at 1 atm. *J. Chem. Eng. Data* **31,** 154–156 (1986).
16. Schimmel, F. A. The Ternary Systems Ferrous Chloride—Hydrogen Chloride—Water, Ferric Chloride—Ferrous Chloride—Water. *J. Am. Chem. Soc.* **74,** 4689–4691 (1952).
17. Ernst, P. & Newman, R. C. Explanation of the effect of high chloride concentration on the critical pitting temperature of stainless steel. *Corros. Sci.* **49,** 3705–3715 (2007).